Supplementary material:
Interaction induced ac-Stark shift of exciton-polaron resonances

I. DEVICE AND ELECTRON DENSITY ESTIMATION

Our device structure is sketch in Fig. 1 of the main text. It consists of a monolayer $MoSe_2$ encapsulated in hBN flakes with a thicknesses estimated from their optical contrast to be $d_{\mathrm{top}} \approx 21 \pm 3\,\mathrm{nm}$ (top layer) and $d_{\mathrm{bot}} \approx 42 \pm 5\,\mathrm{nm}$ (bottom layer). Underneath the lower hBN, a few-layer graphite flake is used as a gate to electrostatically dope the sample. All flakes were mechanically exfoliated from bulk crystals, and stacked using a standard dry-transfer technique [1] with a poly(bisphenol A carbonate) film on a polydimethylsiloxane (PDMS) stamp. The heterostructure was then deposited on a Si/SiO_2 (285 nm) substrate, and the graphite and $MoSe_2$ flakes were then contacted using optical lithography and electron beam metal deposition.

To introduce electrons in the TMD, we ground it while applying a voltage V to the graphite gate. Neglecting the quantum capacitance of the doped TMD monolayer, we obtain the charge density from the relation $n_e e = C(V - V_0)$, where e is the electron charge, V_0 is the gate voltage at the onset of doping and $C = \epsilon_0 \epsilon_{\mathrm{hBN}}^{\perp}/d_{\mathrm{bot}}$ is the geometric capacitance. For the hBN out-of-plane dielectric constant we use the value $\epsilon_{\mathrm{hBN}}^{\perp} = 3.5$ [2, 3]. The assumption of a negligible quantum capacitance has been verified in previous studies of Van der Waals heterostructures, where the charge density could be infered e.g. from the filling of a Moiré superlattice [4–6] or of Landau levels [7]. It is further supported in our sample by the observation of a linear dependence of the AP oscillator strength $f_{AP} \propto (V - V_0)$ at low density (See Sec. IV).

II. EXPERIMENTAL SETUP

The sample is loaded in a dry cryostat (attodry800) with free space optical access. Our main light source is a pulsed Ti:sapphire laser (Tsunami, Spectra-physics), with a repetition rate of 76 MHz and a pulse duration of $\approx 140\,\mathrm{fs}$ (FWHM, before pulse-shaping). The pulses are split into the pump and probe paths, before being recombined, as shown in Fig. 1 of the main text. For the pump beam, we reduce the bandwidth using a pulse-shaper, typically to $\approx 5\,\mathrm{meV}$, resulting in a duration of $\approx 270\,\mathrm{fs}$. We show a typical time profile obtained using an autocorrelator in Fig. S1, from which we can extract the pulse duration using a Gaussian fit.

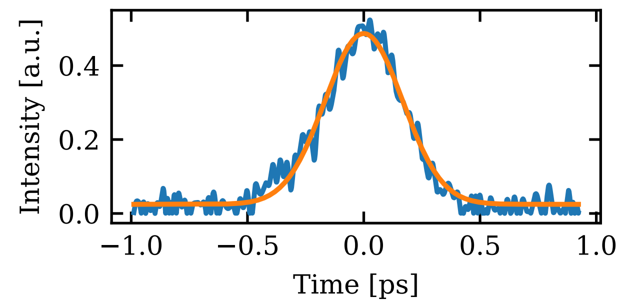

FIG. S1. Time profile of the pump pulse measured using an autorcorrelator. From a Gaussian fit, we obtain a duration of $\approx 270\,\mathrm{fs}$ (FWHM).

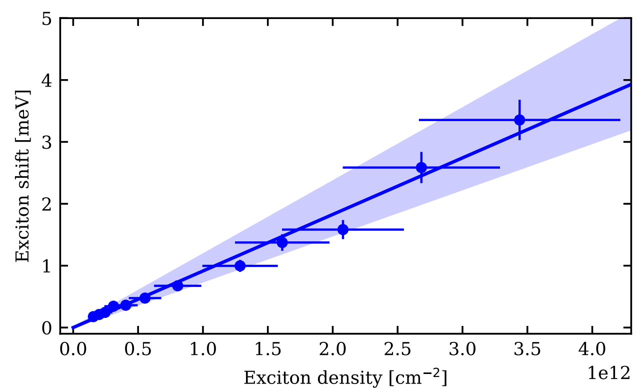

FIG. S2. Exciton energy shift as a function of the density of excitons generated by the pump beam. The y error bars correspond to the statistical error estimated by repeating the measurement 3 times. The x error bars correspond to the systematic error arising from the uncertainty on the various parameters (in particular the exciton (non)radiative decay rate) which are used to estimate the exciton density. The blue line is a linear fit (with the confidence interval shown as a blue cone), from which we extract the interaction strength $U_{\mathrm{ex}} \approx 0.09 \pm 0.03\,\mu\mathrm{eV}\mu\mathrm{m}^2$.

For the probe pulse, we use a non-linear crystal fiber (femtowhite 800, NKT photonics) to generate a broad continuum spanning the exciton/polarons resonances. Both pulses are focused near the diffraction limit onto the sample using a microscope objective with NA≈ 0.8 (LT-APO/VISIR/0.82). We typically use average power of $\sim 10^2\mu$W for the pump and below microwatt for the probe. For the pump, this results in peak intensity of order ~ 1 GW/cm^2, and fluences of order $\sim 10^2$uJ/cm^2.

III. ESTIMATION OF THE EXCITON DENSITY AND INTERACTION STRENGTH

In order to estimate the exciton-exciton interaction strength, we need to evaluate the density of excitons n_{ex}

generated by the pump beam. From the optical Bloch equation, we can relate n_{ex} to the flux of photon I_{i} impinging on the TMD [8]

$$n_{\mathrm{ex}} = \frac{2 I_{\mathrm{i}} R_0}{\gamma_r (1 + \delta_{\mathrm{ex}}^2 / \tilde{\gamma}^2)}\,, \tag{1}$$

where γ_{r} (γ_{nr}) is the (non-)radiative decay rate, $\tilde{\gamma} = (\gamma_{\mathrm{nr}} + \gamma_{\mathrm{r}})/2$ is the dephasing rate and $R_0 = \gamma_{\mathrm{r}}^2/(\gamma_{\mathrm{r}} + \gamma_{\mathrm{nr}})^2$ the TMD reflectance on resonance. From a transfer matrix simulation [8] we obtain $\gamma_{\mathrm{r}} = 2.4 \pm 0.4\,\mathrm{meV}$, $\gamma_{\mathrm{nr}} = 0.6 \pm 0.3\,\mathrm{meV}$, hence $R_0 = 0.65 \pm 0.13$ and we can deduce the field on the TMD (and hence I_{i}) as a function of the incoming field. The error bar comes from the uncertainty on the hBN thicknesses and refractive index (see Sec. I) which are inputs of the TMM simulation.

We show in Fig. S2 the measured exciton light shift Δ as a function of the exciton density. In this measurement the light intensity is kept to a fixed value $I_{\mathrm{peak}} \approx 1.7 \pm 0.3\,\mathrm{GW/cm^2}$ ($\approx 170\,\mathrm{uW}$ average power) and we scan the detuning δ in a range $30 - 110\,\mathrm{meV}$. We observe a linear dependence $\Delta = U_{\mathrm{ex}} n_{\mathrm{ex}}$ and extract the interaction strength from a fit, $U_{\mathrm{ex}} \approx 0.09 \pm 0.03\,\mu\mathrm{eV}\mu\mathrm{m}^2$.

IV. FITTING OF THE REFLECTION DATA

Due to the interference of the light reflected at the different dielectric interfaces of our stack, our reflection spectrum are fitted by a sum of a Lorentzian and a dispersive Lorentzian

$$S(E) = A\left[\cos\theta \frac{\frac{\sigma^2}{2}}{(E - E_0)^2 + \frac{\sigma^2}{4}} + \sin\theta \frac{\sigma(E - E_0)}{(E - E_0)^2 + \frac{\sigma^2}{4}}\right]. \tag{2}$$

Here E is the reflected photon energy, and A, σ, E_0 are fitting parameters which depend on n_{e}. The last fitting parameter θ is independent on n_e; in practice, we let it free and verify that we obtain the same values for all fits. We always fit independently the AP and RP resonance. We show in Fig. S3 the results of the fit as a function of the gate voltage.

In addition we also fit the data with the reflection spectrum predicted by transfer matrix simulation [8], with the AP/RP energy and (non)radiative decay rates taken as fitting parameter. From this analysis, we obtain the ratio of the oscillator strength $f_{\mathrm{AP,RP}}/f_{\mathrm{ex}} = \gamma_{\mathrm{r,AP/RP}}/\gamma_{\mathrm{r,ex}}$, shown in Fig. S3 **d**, which we then use to infer the interaction strength ratio $U_{\mathrm{AP}}/U_{\mathrm{ex}}$ from a measurement of the light shift as described in the main text.

V. COUPLING TO THE BIEXCITON STATE

In this section, we report on our observation of the exciton light shift (at charge neutrality), for cross-circularly polarized pump and probe laser. In this situation, which

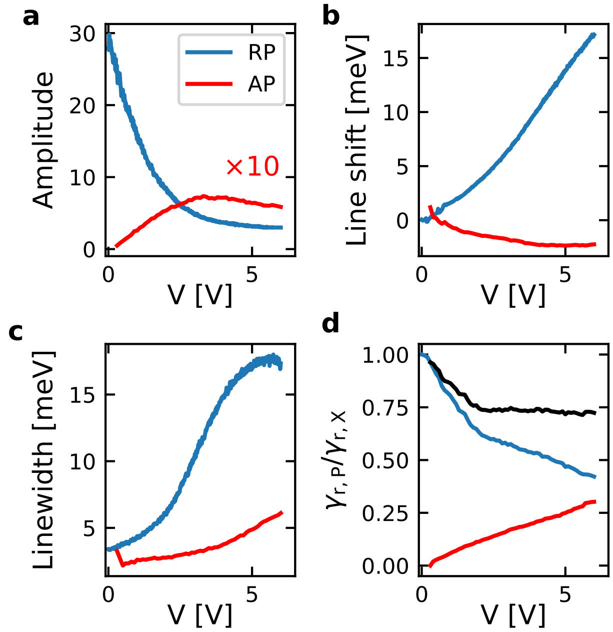

FIG. S3. Results of the fitting of the AP and RP reflection spectrum. We use the fitting function (2). In **a**, **b**, **c**, we show the fitted amplitude $A(V)$ (multiplied by ten for the AP), resonance shift $E_0(V) - E_0(0)$ and linewidth $\sigma(V)$ as a function of the gate voltage V for the AP (red line) and exciton/RP resonance (blue line). The onset of doping occurs at $V_0 \approx 0.35\,\mathrm{V}$. The last panel **d** show $\gamma_{\mathrm{r,AP}}/\gamma_{\mathrm{r,ex}}$ (red) and $\gamma_{\mathrm{r,RP}}/\gamma_{\mathrm{r,ex}}$ (blue), the radiative decay rate of the AP and RP, normalized to that of the exciton. The black line is the sum $(\gamma_{\mathrm{r,AP}} + \gamma_{\mathrm{r,RP}})/\gamma_{\mathrm{r,ex}}$, showing a small decay at low density

has been studied in [9, 10], a new contribution to the light shift arise from the coupling to a biexciton sate, a bound state of two excitons in opposit valleys. The energy level structure to consider is shown in Fig. S4 **a** and in the dressed state basis in **b**. When the pump laser is detuned from the exciton transition by the biexciton binding energy $\delta_{\mathrm{ex}} = E_{\mathrm{binding}}$, we expect an avoided crossing between the dressed states $|X, n\rangle$ and $|XX, n-1\rangle$, where X and XX respectively designate the exciton and biexciton states, and the integers n, $n-1$ corresponds to the number of pump photons [11]. Indeed, we observe a change of sign of the light shift as we sweep the pump-laser detuning across the biexciton resonance $\delta_{\mathrm{ex}} = E_{\mathrm{binding}}$, as shown in Fig. S4 **c**,**d**. The amplitude of the shift always remain much smaller than the exciton linewidth and decrease near resonance, where we mostly observe a broadening of the transition and did not resolve the expected Autler-Towns splitting. From a heuristic fit $\Delta_{\mathrm{ex},\perp} = a \arctan[(\delta_{\mathrm{ex}} - E_{\mathrm{binding}})/b] + c$, of the light shift at zero time delay (panel **c**), we extract the biexciton binding energy $E_{\mathrm{binding}} = 29 \pm 1.5\,\mathrm{meV}$. As mention in the main text, this value is slightly larger than the estimates of [9, 10], which could be due to the presence of residual charges in devices without electrical gates, screening the Coulomb interaction and thereby reducing

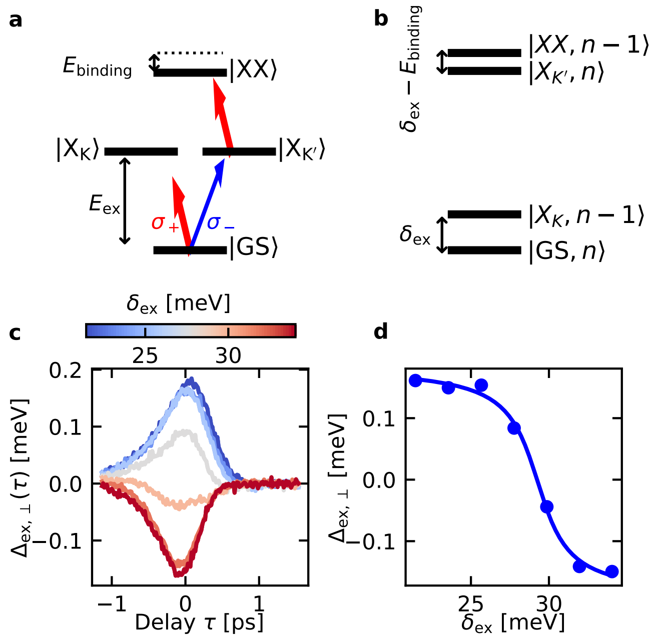

FIG. S4. Exciton light shift in cross-polarization. The relevant energy levels are shown in **a**. The σ_+-polarized pump laser (red arrow) drives the transition between the biexciton state $|XX\rangle$ and the K'-valley exciton $|X_{K'}\rangle$ produced by the σ_--polarized probe laser (blue). Near the resonance $\delta_{ex} \approx E_{\mathrm{binding}}$, the dominant contribution to the light shift of the K'-valley exciton comes from level repulsion between the dressed state $|XX, n-1\rangle$ and $|X_{K'}, n\rangle$, as shown in **b**. This results in a sign change of the light shift $\Delta_{\mathrm{ex},\perp}$, plotted as a function of the pump-probe delay τ in **c**. In **d**, we show the light shift at zero time-delay as a function of the pump detuning, which is fitted (solid blue line) to extract the biexciton binding energy E_{binding}.

the biexciton binding energy.

VI. FIT OF THE LIGHT SHIFT WAVELENGTH DEPENDENCE

In this section we provide more details on the fitting of the light shift Δ_{AP} as a function of the pump detuning. We focus on the analysis of the AP, but the data for the exciton in co-polarization is similar to that of the AP, while the case of cross-polarization is described in Sec. V.

Quite generally, from second order perturbation theory, the light shift can be expanded as [12]

$$\Delta_{\mathrm{AP}} = \frac{A}{\delta_{\mathrm{AP}}} + \frac{B}{\delta_{\mathrm{AP}}^2} + \frac{C}{\delta_{\mathrm{RP}}^2} + \frac{D}{\delta_{\mathrm{AP}} - E_{\mathrm{binding}}}, \qquad (3)$$

where the first term corresponds to the usual ac-Stark shift arising from light-matter dressing, the second and third terms respectively capture the AP-AP and AP-RP interaction, and the last term can arise from a coupling to a charged biexciton.

For the small detunings (compared to the exciton Rydberg) that we investigate, we expect the interaction terms to dominate over the light-matter dressing. Furthermore, we also expect the AP-AP interaction to play a dominant role compared to the AP-RP interaction. Indeed, our pump laser being red-detuned from the AP resonance, we always have $\delta_{\mathrm{AP}} < \delta_{RP}$, and we typically have $n_{\mathrm{AP}} \ll n_{\mathrm{RP}}$. This strong inequality is however not always satisfied, in particular at low density when $f_{\mathrm{AP}} \ll f_{\mathrm{RP}}$. On the other hand, this regime also corresponds to the situation where the exciton content is very large for the RP and conversely very small for the AP, resulting in $U_{\mathrm{AP-AP}} \gg U_{\mathrm{AP-RP}}$. We therefore always expect $C/\delta_{\mathrm{AP}}^2 = U_{\mathrm{AP-AP}} n_{\mathrm{AP}} \gg D/\delta_{\mathrm{RP}}^2 = U_{\mathrm{AP-RP}} n_{\mathrm{RP}}$. Finally, same-valley excitons are not expected to form a stable bound state due to Pauli blocking, and therefore we do not expect the last contribution in (3) to arise for co-circular pump and probe polarization. For cross-circular polarization, at charge neutrality a biexciton exists and we report on his contribution to the AC-Stark shift in Sec. V. In the presence of electrons, charged biexciton have been observed in WS_2 [13]. However, Pauli blocking is inhibiting the formation of a charged biexcion for Molybdenum compounds [9], where the resident electron and that of the exciton occupy the same lower conduction band (contrary to Tungsten compounds, where bright excitons have their electron in the upper conduction band).

From all these considerations, we expect the AP light shift to follow a law $\Delta_{\mathrm{AP}} = B/\delta_{\mathrm{AP}}^2$ in the regimes explored in our work. As shown in Fig. S5, we can recover this result from a fit to our data, without prior knowledge.

First, in panel **a**, we show the case of co-circularly polarized pump-probe. A one-parameter fit B/δ_{AP}^2 captures very well our measurements; the largest deviation from the fit, observed at small detuning, could be due to absorption. In contrast our data cannot be reproduced by a fit in A/δ_{AP} or C/δ_{RP}^2. Finally, in a three parameter fit including these three terms, the AP-AP interaction terms contributes to at least 93% of the light shift (at the largest detuning).

We observe a similar behavior for cross-polarization (up to a sign change of B). In that case, we also attempt a two-parameters fit $D/(\delta_{\mathrm{AP}} - E_{\mathrm{binding}})$, which yields a poor agreement with the data, thereby excluding a possible shift induced by the transition to a charged biexciton state.

VII. SIMULATION OF THE LINE DISTORTION

It can be seen in figure 1 **c** of the main text that the effect of the pump on the exciton resonance is more complex than a bare line shift. We observe (i) a broadening of the resonance and (ii) at negative time delay, the appearance of side peaks, both on the blue and red side of the exciton resonance. In an adiabatic approxi-

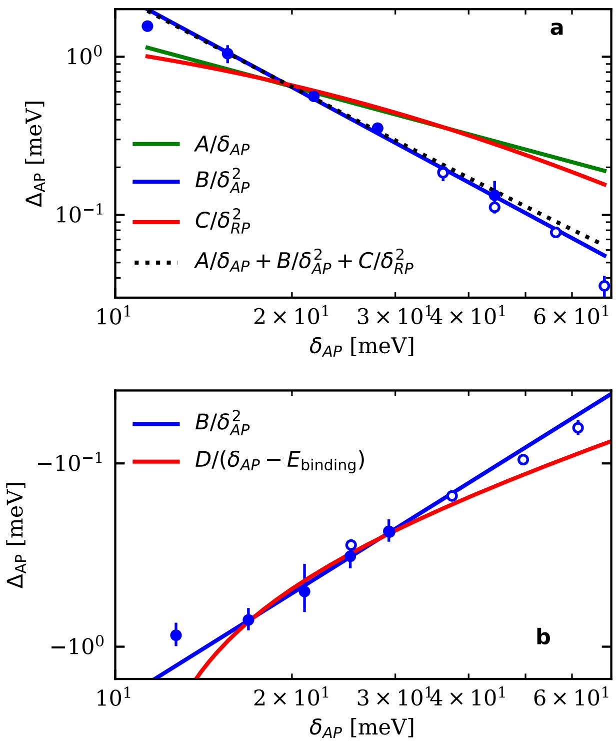

FIG. S5. Fits of the wavelength dependence of the AP light shift, for co- (**a**) and cross- (**b**) circularly pump-probe polarization. In both panel, we combine two data sets, one obtain with low pump intensities (at small detuning, blue filled data points) and one obtained at larger pump intensities (at larger detuning, white filled data points). The latter are then rescaled by the intensity ratio. In this way, we are able to keep a decent signal-to-noise ratio as we increase the detuning, while remaining in the linear-in-intensity regime closer to resonance.

mation, We have an instantaneous and local light shift $\Delta(x,t) \propto I_{\text{pump}}(x,t)$. The duration of the pump pulse is about twice that of the probe pulse, and both beams are focused to the same spot size. These two effects results in an inhomogeneous (in both time and space) light shift, which readily explains (i). As mentioned in the main text, the fact that the resonance almost perfectly recovers excludes non-coherent effects, such as heating or photo doping, as significant broadening mechanisms. The appearance of side peaks (ii) is a more complex but well known artifact of pump-probe experiments, which is studied in details in e.g. [14, 15]. Briefly, the side peaks can be understood as the free induction decay of a real population of exciton injected by the probe and perturbed by the pump - which explains why this effects shows up when the probe comes before the pump, i.e. for $\tau \lesssim 0$. A quantitative treatment requires the resolution of the semiconductor optical Bloch equation beyond the adiabatic approximation. Here, we propose a very simple approach, which can capture the appearance of both

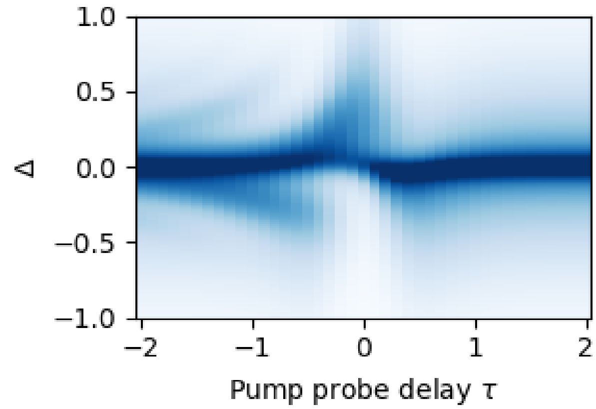

FIG. S6. Simulation of the pump-probe experiments taking into account the finite duration of the laser pulses, which results in a broadening of the resonance and side bands at negative time delay.

blue and red detuned peaks, but which is not meant to be quantitatively accurate. We consider that the polarization generated by the probe pulse read

$$P(t) = \cos\left[(\omega + \Delta_0 g_{\text{pump}}(t)^2)t\right] \times \\ P_0\left[g_{\text{probe}}(t-\tau) + P_1\Theta(t-\tau)\mathrm{e}^{-\gamma(t-\tau)}\right] \quad (4)$$

where g_{pump} (g_{probe}) is the envelope of the pump (probe) electric field, which we take to be the hyperbolic secant function with width σ_{pump} (σ_{probe}). We considered that the pump (probe) pulse arrives at $t = 0$ ($t = \tau$). The free induction decay responsible for the side peaks corresponds to the second term in (4), where Θ is a step function (we take the hyperbolic tangent with width σ_{probe}) and γ corresponds to the exciton decay rate. We Fourier transform $P(t)$ and shows its modulus square in Fig. S6, for $\omega = 2400\,\text{rad.ps}^{-1}$; $\Delta_0/\omega = 2 \times 10^{-3}$; $\sigma_{\text{pump}} = 0.4\,\text{ps}$; $\sigma_{\text{probe}} = 0.1\,\text{ps}$; $P_1/P_0 = 0.1$; $\gamma = 1.4\,\text{ps}^{-1}$. These parameters are not determine after a precise calibration, there chosen are in a realistic range to observe clear side peaks, as can be seen in Fig. 4. In particular we have chosen $\sigma_{\text{probe}}/\sigma_{\text{pump}}$ slightly smaller than in the actual experiments, for the purpose of having brighter side peaks.

To conclude we point out that these artifact are more pronounced for the exciton resonance, compared of the AP. This could be due to a smaller ratio P_1/P_0 for the AP.

VIII. REPULSIVE POLARON LIGHT SHIFT

In the main text we focused our analysis of the AC-Stark shift of the attractive polaron. Here we breifly discuss the case of the repulsive polaron (RP).

Similarly to the exciton or AP, we observe a blue shift of the RP for co-circularly polarized pump and probe

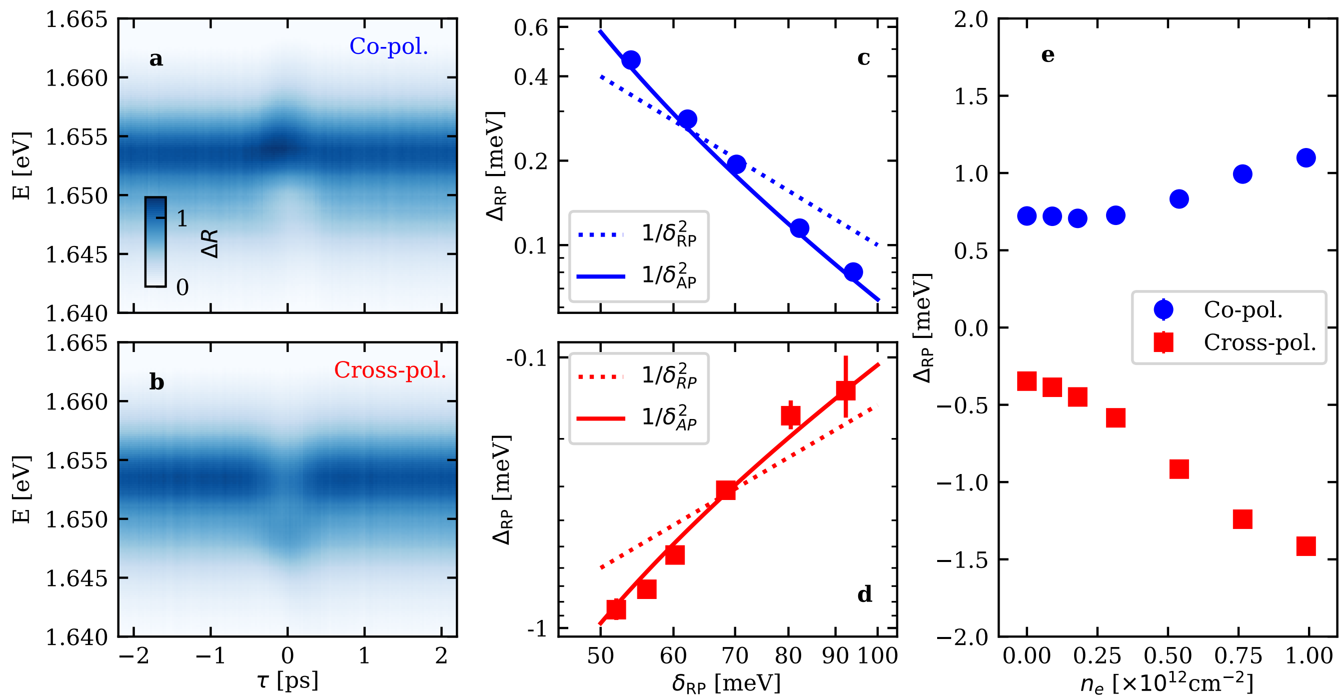

FIG. S7. **Repulsive polaron light shift**. Evolution of the reflection spectrum as a function of the pump-probe delay, in co- (**a**) and cross-circular polarization (**b**). At these relatively large electronic density $n_e \approx 10^{12}\mathrm{cm}^{-2}$, the detuning dependance of the light shift (**c** and **d**) is better fitted by a $1/\delta_{AP}^2$ instead of $1/\delta_{RP}^2$. This observation indicates that AP-RP interactions are the leading contribution to the light shift in the detuning range explored here. This effect, together with an overall increase of the interaction due to the polaronic dressing, contributes to an increase of the light shift with the electronic density (**e**). These data were obtained in the same experimental condition as for the AP light shift shown in Fig. 3 and 4 of the main text, i.e. with $I_{\mathrm{pk}} \approx 1.7\,\mathrm{GW\,cm}^{-2}$ and $\delta_{\mathrm{AP}} \approx 25\,\mathrm{meV}$, $\delta_{\mathrm{RP}} \approx 50\,\mathrm{meV}$, (note that these are the detuning at $n_e \to 0$, they slightly change with increasing n_e, see Fig. S3 **b**).

pulse, and a red shift for cross-circular polarization, see Fig. S7 **a**,**b**. The former is driven by repulsive interaction, as described for the exciton or AP. The latter can have two origins, the coupling to the biexciton (discussed in Sec. V), in particular at low densities when the exciton content of the RP is large and attractive interaction (as observed for the AP) at larger densities when the polaronic dressing is more prominent. In that second situation, due to the transfer of oscillator strength from the RP to the AP for increasing n_e (see Fig. S3), both RP-RP and AP-RP interactions should be taken into account:

$$\Delta_{\mathrm{RP}} = U_{\mathrm{RP-RP}} n_{\mathrm{RP}} + U_{\mathrm{AP-RP}} n_{\mathrm{AP}}\,. \tag{5}$$

The role of AP-RP interaction is further enhanced for a red-detuned pump, such that $\delta_{\mathrm{AP}} < \delta_{\mathrm{RP}}$. The relative contribution of the RP-RP and AP-RP interaction can be deduced from the dependence of the light shift on the pump detuning. We observe in Fig. S7 **c d**, that for both co- and cross-polarization, the RP light shift is indeed better fitted by a $1/\delta_{AP}^2 \propto n_{\mathrm{AP}}$ law instead of $1/\delta_{RP}^2 \propto n_{\mathrm{RP}}$, showing that at such electronic density $n_e \approx 10^{12}\mathrm{cm}^{-2}$, the AP-RP interactions are the leading contribution to the light shift. For increasing electronic density, the enhancement of the interaction counter-acts the reduction of the oscillator strength and we observe an increase of the light shift in both polarization (Fig. S7 **e**). Note that we restricted our analysis to densities $n_e \lessapprox 10^{12}\,\mathrm{cm}^{-2}$ as the RP resonance becomes too broad for larger densities and the fit unreliable.

[1] P. Zomer, M. Guimarães, J. Brant, N. Tombros, and B. Van Wees, Applied Physics Letters **105**, 013101 (2014).

[2] A. Laturia, M. L. Van de Put, and W. G. Vandenberghe, npj 2D Materials and Applications **2**, 6 (2018).

[3] K. K. Kim, A. Hsu, X. Jia, S. M. Kim, Y. Shi, M. Dresselhaus, T. Palacios, and J. Kong, ACS nano **6**, 8583 (2012).

[4] E. C. Regan, D. Wang, C. Jin, M. I. B. Utama, B. Gao, X. Wei, S. Zhao, W. Zhao, Z. Zhang, K. Yumigeta, M. Blei, J. D. Carlström, K. Watanabe, T. Taniguchi, S. Tongay, M. Crommie, A. Zettl, and F. Wang, Nature **579**, 359 (2020).

[5] Y. Tang, L. Li, T. Li, Y. Xu, S. Liu, K. Barmak, K. Watanabe, T. Taniguchi, A. H. MacDonald, J. Shan, and K. F. Mak, Nature **579**, 353 (2020).

[6] Y. Shimazaki, I. Schwartz, K. Watanabe, T. Taniguchi, M. Kroner, and A. Imamoğlu, Nature **580**, 472 (2020).

[7] T. Smoleński, O. Cotlet, A. Popert, P. Back, Y. Shimazaki, P. Knüppel, N. Dietler, T. Taniguchi, K. Watanabe, M. Kroner, and A. Imamoglu, Phys. Rev. Lett. **123**, 097403 (2019).

[8] G. Scuri, Y. Zhou, A. A. High, D. S. Wild, C. Shu, K. De Greve, L. A. Jauregui, T. Taniguchi, K. Watanabe, P. Kim, *et al.*, Physical review letters **120**, 037402 (2018).

[9] K. Hao, J. F. Specht, P. Nagler, L. Xu, K. Tran, A. Singh, C. K. Dass, C. Schüller, T. Korn, M. Richter, *et al.*, Nature communications **8**, 15552 (2017).

[10] C.-K. Yong, J. Horng, Y. Shen, H. Cai, A. Wang, C.-S. Yang, C.-K. Lin, S. Zhao, K. Watanabe, T. Taniguchi, *et al.*, Nature Physics **14**, 1092 (2018).

[11] C. Cohen-Tannoudji and S. Reynaud, Journal of Physics B: Atomic and Molecular Physics **10**, 345 (1977).

[12] M. Combescot, Physics reports **221**, 167 (1992).

[13] J. B. Muir, J. Levinsen, S. K. Earl, M. A. Conway, J. H. Cole, M. Wurdack, R. Mishra, D. J. Ing, E. Estrecho, Y. Lu, *et al.*, Nature Communications **13**, 6164 (2022).

[14] S. Koch, N. Peyghambarian, and M. Lindberg, Journal of Physics C: Solid State Physics **21**, 5229 (1988).

[15] H. Haug and S. W. Koch, *Quantum theory of the optical and electronic properties of semiconductors* (World Scientific Publishing Company, 2009).